

Energetics of a Single Qubit Gate

J. Stevens¹,¹ D. Szombati,¹ M. Maffei,² C. Elouard³,³ R. Assouly¹,¹ N. Cottet¹,¹ R. Dassonneville¹,¹ Q. Ficheux,¹ S. Zeppetbauer¹,¹ A. Bienfait,¹ A. N. Jordan,^{4,5} A. Auffèves,² and B. Huard¹

¹*Ecole Normale Supérieure de Lyon, CNRS, Laboratoire de Physique, F-69342 Lyon, France*

²*CNRS and Université Grenoble Alpes, Institut Néel, F-38042 Grenoble, France*

³*QUANTIC team, INRIA de Paris, 2 Rue Simone Iff, 75012 Paris, France*

⁴*Institute for Quantum Studies, Chapman University, 1 University Drive, Orange, California 92866, USA*

⁵*Department of Physics and Astronomy, University of Rochester, Rochester, New York 14627, USA*

 (Received 21 October 2021; revised 19 August 2022; accepted 24 August 2022; published 9 September 2022)

Qubits are physical, a quantum gate thus not only acts on the information carried by the qubit but also on its energy. What is then the corresponding flow of energy between the qubit and the controller that implements the gate? Here we exploit a superconducting platform to answer this question in the case of a quantum gate realized by a resonant drive field. During the gate, the superconducting qubit becomes entangled with the microwave drive pulse so that there is a quantum superposition between energy flows. We measure the energy change in the drive field conditioned on the outcome of a projective qubit measurement. We demonstrate that the drive's energy change associated with the measurement backaction can exceed by far the energy that can be extracted by the qubit. This can be understood by considering the qubit as a weak measurement apparatus of the driving field.

DOI: [10.1103/PhysRevLett.129.110601](https://doi.org/10.1103/PhysRevLett.129.110601)

Understanding the energetic resources needed to operate quantum computers is crucial to assess their performance limitations [1–10]. Beyond the fundamental costs associated with information processing [11], e.g., reset [12] and measurements [13,14], quantum gates need energy to manipulate qubits encoded in nondegenerate states [10,15]. Since a gate can prepare a quantum superposition of states with different energies, the energy balance between the gate controller and the qubit can be seen as a quantum superposition of energetic costs. Focusing on gates performed by resonant driving, the drive appears to have exchanged energy with the qubit. Yet the amount of transferred energy is undetermined until the qubit state is measured. How is the energy in the driving mode modified by the qubit measurement and what does it reveal about the qubit-drive system? Superconducting circuits offer a state-of-the-art platform for exploring this question owing to the possibility to perform single shot qubit readout using an ancillary cavity and quantum-limited measurements of propagating microwave modes [16]. In particular, it is possible to manipulate [17–20] and probe [21–24] the fields interacting resonantly with the qubit. Superconducting circuits have thus been useful to explore quantum thermodynamics properties of their spontaneous or stimulated emission [25–28], and build quantum thermal engines [29–31]. Correlations between the resonant drive amplitude and the outcome of a later qubit measurement have been evidenced by probing quantum trajectories of superconducting qubits [32–36] including when a projective measurement is used to perform postselection

[37–39]. However, the demonstration of correlations between the energy of the drive mode and the qubit state is missing.

In this Letter, we present an experiment in which we directly probe the energy in the driving mode conditioned on the measured qubit state. We observe that measuring the qubit energy leads to a change in the energy of the driving pulse owing to its entanglement with the qubit before measurement. Strikingly, we also observe that the energy of the pulse can change by more than a quantum depending on the measured qubit state, revealing a subtle backaction of the qubit measurement on the drive pulse.

In order to better understand the rise of these correlations, let us consider the joint evolution of the qubit and drive mode during the qubit gate. Assuming the qubit starts in the ground state $|g\rangle$, and is driven by a coherent state $|\psi_{\text{in}}\rangle$, the qubit and the propagating drive mode a are initially in the separable state $|\psi_{\text{in}}\rangle \otimes |g\rangle$ [see Fig. 1(a)]. Owing to the light-matter coupling between the drive mode and the qubit, they evolve into the entangled state [3,40,41]

$$\lambda_g |\psi_g\rangle \otimes |g\rangle + \lambda_e |\psi_e\rangle \otimes |e\rangle \quad (1)$$

where λ_g and λ_e are the probability amplitudes for each state in the superposition, and $|\psi_{g,e}\rangle$ designate the outgoing states of the drive mode [see Fig. 1(b)]. Note that these parameters and states depend on $|\psi_{\text{in}}\rangle$ implicitly. The qubit gate is parametrized by the rotation of angle θ undergone by the qubit Bloch vector, revealed by tracing over the field. Interestingly, the entanglement above limits the fidelity of a

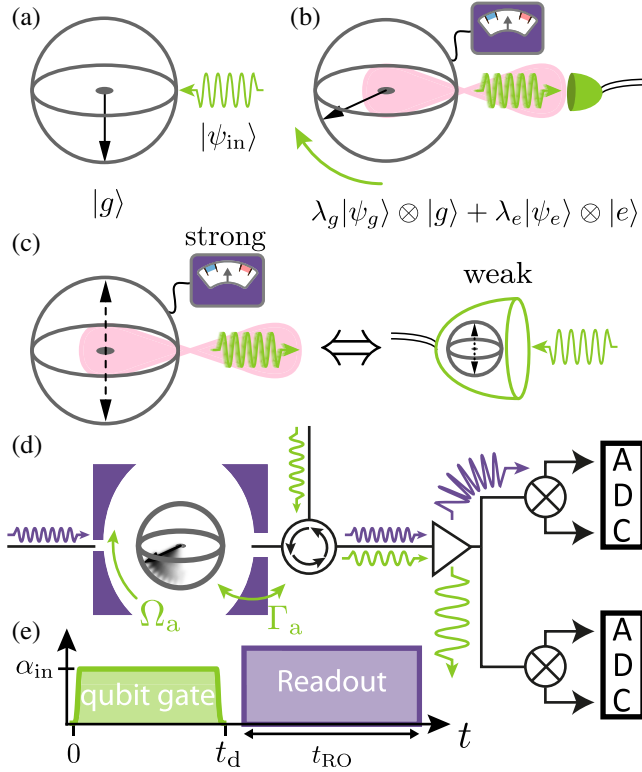


FIG. 1. Principle of the experiment. (a) Coherent wave packet $|\psi_{\text{in}}\rangle$ (green arrow) at the qubit frequency interacts with a qubit prepared in $|g\rangle$ (Bloch vector). (b) Resulting entangled state Eq. (1). The energy of the outgoing drive wave packet is measured and averaged conditionally on the outcome of a strong readout of the qubit energy. (c) Schematics highlighting the equivalence between the action of the projective qubit measurement and that of a weak measurement apparatus on the pulse. (d) The transmon qubit is placed inside a microwave cavity (purple) to perform its readout by sending a pulse at the cavity frequency through a weakly coupled port (left). The resonant field (green) addressing the qubit is sent through a strongly coupled port on the right. Both pulses exit through this port and are directed by a circulator into low noise amplifiers. Their quadratures are measured via two heterodyne setups based on analog-to-digital converters (ADCs) operating at qubit and cavity frequencies. (e) Scheme of the experimental pulse sequence, where $t_d = 400$ ns and $t_{\text{RO}} = 704$ ns [47].

qubit gate, a question which has been at the core of an intense two decades old debate [2–4,7,40,42–45], since the purity of the qubit density matrix ρ reads

$$\text{tr}(\rho^2) = 1 - 2|\lambda_g\lambda_e|^2(1 - |\langle\psi_e|\psi_g\rangle|^2). \quad (2)$$

Luckily for quantum computing, it is possible to reach large gate fidelity since the minimum gate error $1 - \text{tr}(\rho^2)$ scales as the inverse of the average photon number in $|\psi_{\text{in}}\rangle$ [1,3,40,46]. The lack of purity also determines how much information can be extracted about the drive mode when measuring the qubit state. When the qubit is measured, the

measurement backaction prepares the drive mode a in states of different energy expectations. Conservation of the expected energy before and after the resonant interaction leads to the following equality relating the expected number of quanta in the initial state $|\psi_{\text{in}}\rangle \otimes |g\rangle$ and the final state (1):

$$\langle\hat{a}^\dagger\hat{a}\rangle_{|\psi_{\text{in}}\rangle} = |\lambda_g|^2\langle\hat{a}^\dagger\hat{a}\rangle_{|\psi_g\rangle} + |\lambda_e|^2[\langle\hat{a}^\dagger\hat{a}\rangle_{|\psi_e\rangle} + 1]. \quad (3)$$

In this Letter, we directly measure the energy contained in the states $|\psi_g\rangle$ and $|\psi_e\rangle$, and its dependence on the drive amplitude. Interestingly, from the point of view of the driving mode, the qubit acts as a weak measurement apparatus, which exerts a backaction that our experiment is able to probe [Fig. 1(c)].

Our setup is schematically represented in Fig. 1(d) [47]. A transmon qubit of frequency $\omega_Q = 2\pi \times 4.81$ GHz is embedded in a superconducting cavity of frequency $\omega_R = 2\pi \times 7.69$ GHz below 15 mK. The qubit relaxation time $T_1 = 5.5 \pm 0.3$ μs is mainly limited by its coupling rate $\Gamma_a = 2\pi \times 20$ kHz to a transmission line that carries the driving mode a . The qubit pure dephasing time is $T_\varphi = 2.4$ μs .

We perform the following experiment. First, a pulse of varying amplitude α_{in} , whose phase is chosen so that $\alpha_{\text{in}} > 0$, drives the qubit at frequency ω_Q for a fixed duration $t_d = 400$ ns [Fig. 1(e)]. The pulse is reflected and amplified using a traveling-wave parametric amplifier (TWPA) [52]. A heterodyne measurement yields a continuous record of its two quadratures. This drive pulse induces a rotation of the qubit of angle θ around σ_y . The qubit is then measured dispersively 20 ns later using a 704 ns-long pulse at the cavity frequency ω_R sent on a weakly coupled auxiliary port. This readout pulse exits through the strongly coupled output port used for driving the qubit and its transmission is detected through the same amplification chain.

We start by measuring the average energy in the reflected drive pulse. From the heterodyne measurement it is possible to access both the complex amplitude α_m and the instantaneous outgoing power \dot{n}_m (in units of photons per second) referred to the qubit output port [47]. To account for the added noise of the amplifiers and possible experimental gain drifts, we interleave the measurement with a calibration sequence where the qubit is shifted out of resonance using the ac-Stark effect. The average measured photon flux outgoing from the qubit in state ρ is given by [53–55]

$$\overline{\dot{n}_m}^\rho = \alpha_{\text{in}}^2 - \frac{\Omega_a}{2}\langle\hat{\sigma}_x\rangle_\rho + \Gamma_a \frac{1 + \langle\hat{\sigma}_z\rangle_\rho}{2} \quad (4)$$

where $\Omega_a = 2\sqrt{\Gamma_a}\alpha_{\text{in}}$ denotes the Rabi frequency and $\hat{\sigma}_{x,y,z}$ are the three Pauli matrices. In Fig. 2(a), we show the evolution of $\overline{\dot{n}_m}^\rho$ for varying input drive powers. This

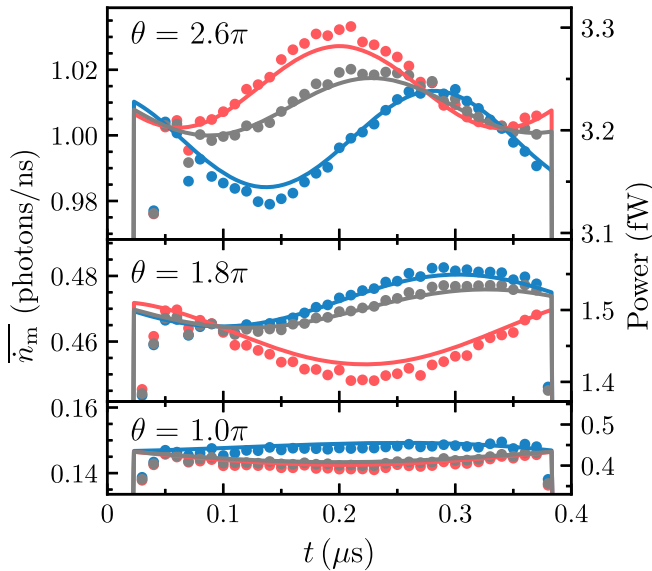


FIG. 2. Measured $\overline{n_m}$ power of the reflected drive. Dots: mean instantaneous power $\overline{n_m}$ of the outgoing drive in units of photon flux [47] as a function of time t . Each panel corresponds to a different input drive amplitude resulting in qubit rotation angles $\theta = \pi, 1.8\pi$, and 2.6π . Gray: averaging without postselection, blue (red): averaging conditioned on the qubit being measured in $|g\rangle$ ($|e\rangle$). Lines: expected power from Eq. (6). The time delay between the experimental and numerical data has been adjusted by hand.

temporal version of the Mollow triplet was already observed in several experiments [21–24].

To extract the correlation between the power of the reemitted microwave drive and final qubit state, we average the instantaneous power conditioned on the measured qubit state (Fig. 2). We observe that a clear deviation exists from the unconditional average power. Theoretically, it is possible to capture the dependence of the drive power on qubit measurement outcome using the past quantum state formalism [56–58]. A full description of the drive mode at each moment in time can be given by considering both the initial starting condition via the density matrix of the qubit $\rho(t)$ and the final measurement result through the effect matrix of the qubit $E(t)$. The density matrix obeys the standard Lindblad equation while the effect matrix is constrained by its value at the final measurement time and is backpropagated using the adjoint of the Lindblad equation (see Ref. [47]). This formalism was used in Ref. [37] in order to determine the postselected average evolution of the transmitted drive amplitude through a qubit. For a reflected drive, the postselected average measured drive amplitude reads

$$\overline{\alpha_m}^{E,\rho} = \alpha_{\text{in}} - \sqrt{\Gamma_a} \text{Re}[E\langle\hat{\sigma}_-\rangle_\rho], \quad (5)$$

where $E\langle\hat{\sigma}_-\rangle_\rho = \{\text{Tr}[E(t)\hat{\sigma}_-\rho(t)]/\text{Tr}[E(t)\rho(t)]\}$ is the weak value of the qubit lowering operator $\hat{\sigma}_- = (\hat{\sigma}_x - i\hat{\sigma}_y)/2$ [37]. The coherent part of the power emitted by the qubit

corresponds to the modulus square of that amplitude. In contrast, in this Letter we are concerned with the total energy contained in the drive mode, and not only the coherent part. One can show that the postselected expectation value of the outgoing photon flux is given by [59,60]

$$\overline{\dot{n}_m}^{E,\rho} = |\alpha_{\text{in}}|^2 - \Omega_a \text{Re}[E\langle\hat{\sigma}_-\rangle_\rho] + \Gamma_a \frac{\text{Tr}[E\hat{\sigma}_-\rho\hat{\sigma}_+]}{\text{Tr}[E\rho]}, \quad (6)$$

where the last term is the weak value of a photodetection rate. To compute Eq. (6), we solve the forward and backward Lindblad equations. An independent measurement allows us to set $\rho(0)$ to a thermal state with an excitation probability 0.088 ± 0.002 . The effect matrix E is set at measurement time $t = t_d$ conditionally on the postselected readout outcome. When the qubit is measured in state $|e\rangle$ with a readout fidelity $F_e = 0.867 \pm 0.028$, it is given by $E_e(t_d) = F_e|e\rangle\langle e| + (1 - F_e)|g\rangle\langle g|$, while, when the qubit is measured in state $|g\rangle$ with a readout fidelity $F_g = 0.985 \pm 0.015$, it is $E_g(t_d) = F_g|g\rangle\langle g| + (1 - F_g)|e\rangle\langle e|$ [47]. Note that without postselection, the effect matrix is the identity and Eq. (6) comes down to the nonpostselected case in Eq. (4). The Eq. (6) reproduces the measured postselected instantaneous powers we observe (solid lines Fig. 2), where the single fit parameter is the electrical delay of the setup.

Our original motivation is to quantify the difference of energy between the postselected drive pulses. The total number of photons contained in the pulse can be calculated as $\langle n_{\text{out}} \rangle = \int_0^{t_d} \overline{\dot{n}_m}^{E,\rho} dt$ from the experimental data. In Fig. 3(a), we show the square root of the measured total photon numbers $\sqrt{\langle n_{\text{out}} \rangle}$ as a function of the rotation angle θ in the Bloch sphere. The photon number scales as the square of the rotation angle as expected since the Rabi frequency scales as the drive amplitude. The observed difference between $\langle n_{\text{out}} \rangle$ for both qubit measurement outcomes is negligible compared to the total number of photons in the pulse, as expected from the strong overlap of states $|\psi_g\rangle$ and $|\psi_e\rangle$.

To reveal the difference between the energies of these states, we thus subtract the mean number of photons contained in the incoming pulse $n_{\text{in}} = \int_0^{t_d} |\alpha_{\text{in}}(t)|^2 dt$ [Fig. 3(b)]. Without postselection, the difference $\Delta n = \langle n_{\text{out}} \rangle - n_{\text{in}}$ oscillates between -1 and 0 , as expected from the principle of energy conservation: when the qubit is excited, it extracts a photon from the pulse and when it is in the ground state the pulse energy stays unchanged. Note that this average loss of one photon owing to energy conservation is not necessarily enforced by the application of the annihilation operator, which could even lead to an increase of the photon number for well chosen quantum states [61]. As commonly observed with weak value measurements, the oscillation amplitudes of the postselected $\Delta n_{g,e}$ can exceed the nonpostselected amplitude [blue and red dots compared to shaded area in Fig. 3(b)] [62]. The postselected photon number Δn_g oscillates in counterphase with Δn_e : the information acquired on the

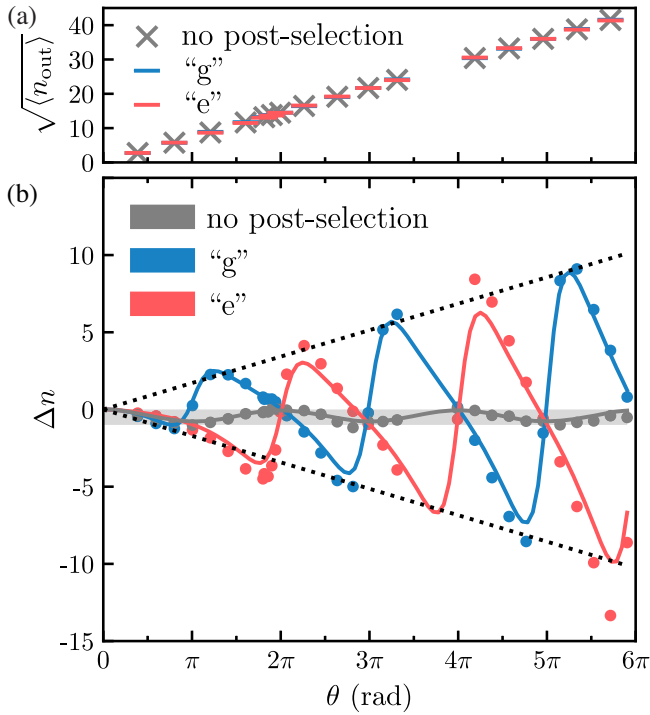


FIG. 3. (a) Square root of the measured total mean number of photons in the outgoing drive pulse as a function of the qubit rotation angle θ around $\hat{\sigma}_y$, for postselected and nonpostselected data. For these photon numbers, the effect of postselection is almost indistinguishable. (b) Dots: measured difference Δn between the mean postselected number of photons and the mean number of photons in the incoming drive pulse as a function of the qubit rotation angle. Colors indicate the kind of postselection. Lines: time integrated Eq. (6). Dotted lines: guides to the eye scaling with $\theta \propto \sqrt{n_{\text{in}}}$. Shaded area: allowed range of exchanged energy without postselection (between -1 and 0 photons).

qubit state distorts the probability of finding a given photon number in the drive pulse.

To better understand the effect of the qubit measurement on the photon distribution, we consider a toy model where the drive pulse is modeled as a stationary harmonic oscillator, which interacts with a decoherence-free qubit for a time t_d at a fixed rate Γ_a [63]. A complete description would treat the drive pulse as a propagating field [43,59,64] and yields identical results. The oscillator starts in a coherent state $|\sqrt{n_{\text{in}}}\rangle = |\theta/\sqrt{4\Gamma_a t_d}\rangle$ with a Poisson distribution $\mathbf{P}_\theta(n)$ for the photon number centered on n_{in} (grey lines in Fig. 4). Postselecting on a particular qubit measurement outcome distorts this probability distribution. The measurement operators \hat{M}_g and \hat{M}_e describing the backaction exerted on the oscillator when the qubit is measured in $|g\rangle$ or in $|e\rangle$ read $\hat{M}_g = \cos(\sqrt{4\Gamma_a t_d} \hat{a}^\dagger \hat{a})$ and $\hat{M}_e = \hat{e} \sin(\sqrt{4\Gamma_a t_d} \hat{a}^\dagger \hat{a})$, where $\hat{e} = \sum_n |n\rangle\langle n+1|$ is the bare lowering operator (see Ref. [47]). Inspired by the problem of photodetection of a cavity output [47], we distinguish two effects in the backaction: (i) the Bayesian

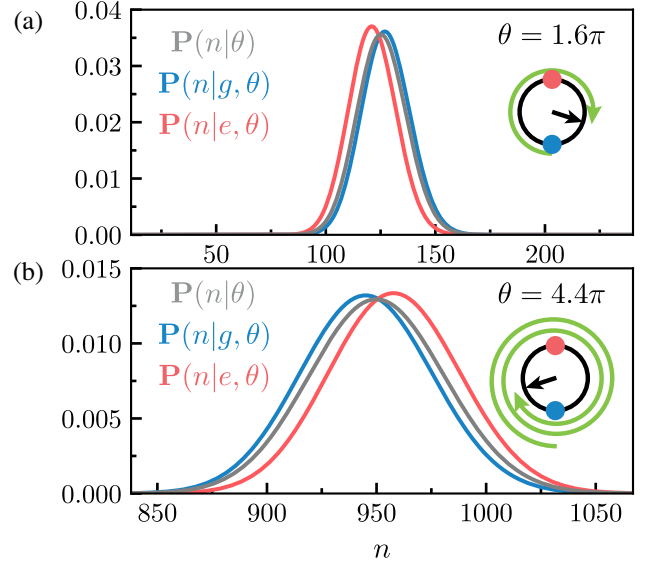


FIG. 4. Probability distribution that the drive pulse contains n photons knowing that it was prepared in a coherent state leading to a Rabi rotation of $\theta = 1.6\pi$ (a) or $\theta = 4.4\pi$ (b). Colors encode the postselected outcome of the qubit measurement: no postselection (grey), $|g\rangle$ (blue), and $|e\rangle$ (red). Insets: Bloch representation of the qubit state after the drive pulse has left it. Green arrow: Rabi rotation. Blue and red dots: $|g\rangle$ and $|e\rangle$ states.

update on the photon distribution conditioned on the measurement outcome and (ii) the extraction of a single photon from the drive pulse which is used to flip the qubit into its excited state.

Through (i), the Poisson distribution is multiplied by $\langle n|\hat{M}_i^\dagger \hat{M}_i|n\rangle$, which is either $\cos^2(\sqrt{n\Gamma_a t_d})$ or $\sin^2(\sqrt{n\Gamma_a t_d})$, and then renormalized (see section IX in [47]). This Bayesian update leads to an increase or a decrease of the mean occupancy [65,66]. The direction depends on the rotation angle since the outcome of the qubit measurement indicates that the qubit is either ahead of its average evolution (more photons than expected in the drive), or behind (less photons). One can see that for $\theta = 1.6\pi$, finding the qubit in $|g\rangle$ projects it ahead of its average evolution and thus offsets the probability distribution $\mathbf{P}_\theta(n|g)$ towards larger photon numbers. Each half turn, the situation reverses, explaining why for $\theta = 4.4\pi$, $\mathbf{P}_\theta(n|g)$ is offset towards smaller photon numbers. This behavior explains the oscillations we observe in Fig. 3. Moreover, owing to the increasing standard deviation of the Poisson distribution $\mathbf{P}_\theta(n)$ with the amplitude $\sqrt{n_{\text{in}}} \propto \theta$, the backaction on Δn increases linearly with θ (dotted lines in Fig. 3(b) and [47]).

Through (ii), the qubit measurement backaction entails the destruction of a photon in the drive pulse when the qubit is found in $|e\rangle$ and no extra cost when in $|g\rangle$. This single photon offset corresponds to the operator \hat{e} in \hat{M}_e and amounts to the minimum of the measured oscillations in the nonpostselected average Δn . For the postselected cases,

this contribution of the measurement backaction is not immediately visible in the measured $\Delta n_{g,e}$, but can be made explicit in the predicted oscillations derived from the past quantum state model of Fig. 3(b) (see Ref. [47]).

In conclusion, we measured the energy flows between a qubit and the resonant drive commonly used to perform single-qubit gates. The unavoidable entanglement between the qubit and the drive reflects on an observable energy exchange. In this context, the projective measurement of the qubit can be understood as a weak measurement of the drive pulse. The experiment is therefore able to clearly demonstrate a correlation between the propagating driving pulse and the qubit, which eventually sets an upper bound on the gate fidelity. Ultimately, the kind of measurements we performed illustrate the limitations set by energy conservation on gate fidelity [45]. The energy change of the drive pulse resulting from the qubit measurement can even exceed the maximal qubit extracted energy of one photon. While surprising when considering the average experiment, it is well explained by a weak-value model. Looking forward, it would be interesting to perform a full quantum tomography of the drive state using newly developed itinerant mode detectors [67,68] by first displacing the quantum state towards low photon numbers, similarly to the steady state case explored in Ref. [28]. We indeed expect the driving mode to be in a controllable non-Gaussian state. Using a squeezed drive would also enable us to quantify the amount of entanglement between qubit and drive that is qubit state dependent [69] and even suppress it fully [70]. From a thermodynamic point of view, this measurement backaction on the energy is at the core of the class of quantum thermodynamic engines that are powered by measurements instead of heat bath [71–81]. Finally, we note that our Letter can be recast in the framework of quantum batteries [82–88]. From that perspective, we realized the anatomy of a charging event for a single qubit battery.

This research was supported by Grant No. FQXi-IAF19-05 from the Foundational Questions Institute Fund, a donor advised fund of Silicon Valley Community Foundation, the Fondation Del Duca, the Templeton World Charity Foundation, Inc (Grant No. TWCF0338), the ANR Research Collaborative Project “Qu-DICE” (ANR-PRC-CES47) and the John Templeton Foundation Grant No. 61835. We acknowledge IARPA and Lincoln Labs for providing a Josephson traveling-wave parametric amplifier. We thank Igor Dotsenko for his useful feedback.

J. S. and D. S. contributed equally to this work.

-
- [1] J. P. Barnes and W. S. Warren, Decoherence and programmable quantum computation, *Phys. Rev. A* **60**, 4363 (1999).
 [2] J. Gea-Banacloche, Some implications of the quantum nature of laser fields for quantum computations, *Phys. Rev. A* **65**, 022308 (2002).

- [3] J. Gea-Banacloche, Minimum Energy Requirements for Quantum Computation, *Phys. Rev. Lett.* **89**, 217901 (2002).
 [4] M. Ozawa, Conservative Quantum Computing, *Phys. Rev. Lett.* **89**, 057902 (2002).
 [5] T. Karasawa and M. Ozawa, Conservation-law-induced quantum limits for physical realizations of the quantum NOT gate, *Phys. Rev. A* **75**, 032324 (2007).
 [6] D. J. Bedingham and O. J. E. Maroney, The thermodynamic cost of quantum operations, *New J. Phys.* **18**, 113050 (2016).
 [7] J. Ikonen, J. Salmilehto, and M. Möttönen, Energy-efficient quantum computing, *npj Quantum Inf.* **3**, 17 (2017).
 [8] Y. Guryanova, N. Friis, and M. Huber, Ideal projective measurements have infinite resource costs, *Quantum* **4**, 222 (2020).
 [9] V. Cimini, S. Gherardini, M. Barbieri, I. Gianani, M. Sbroscia, L. Buffoni, M. Paternostro, and F. Caruso, Experimental characterization of the energetics of quantum logic gates, *npj Quantum Inf.* **6**, 96 (2020).
 [10] S. Deffner, Energetic cost of Hamiltonian quantum gates, *Europhys. Lett.* **134**, 40002 (2021).
 [11] P. Faist, F. Dupuis, J. Oppenheim, and R. Renner, The minimal work cost of information processing, *Nat. Commun.* **6**, 7669 (2015).
 [12] D. Reeb and M. M. Wolf, An improved Landauer principle with finite-size corrections, *New J. Phys.* **16**, 103011 (2014).
 [13] T. Sagawa and M. Ueda, Minimal Energy Cost for Thermodynamic Information Processing: Measurement and Information Erasure, *Phys. Rev. Lett.* **102**, 250602 (2009).
 [14] M. H. Mohammady and A. Romito, Conditional work statistics of quantum measurements, *Quantum* **3**, 175 (2019).
 [15] M. Aifer and S. Deffner, From quantum speed limits to energy-efficient quantum gates, *New J. Phys.* **24**, 055002 (2022).
 [16] X. Gu, A. F. Kockum, A. Miranowicz, Y.-x. Liu, and F. Nori, Microwave photonics with superconducting quantum circuits, *Phys. Rep.* **718–719**, 1 (2017).
 [17] A. A. Houck, D. I. Schuster, J. M. Gambetta, J. A. Schreier, B. R. Johnson, J. M. Chow, L. Frunzio, J. Majer, M. H. Devoret, S. M. Girvin, and R. J. Schoelkopf, Generating single microwave photons in a circuit, *Nature (London)* **449**, 328 (2007).
 [18] I.-C. Hoi, C. M. Wilson, G. Johansson, T. Palomaki, B. Peropadre, and P. Delsing, Demonstration of a Single-Photon Router in the Microwave Regime, *Phys. Rev. Lett.* **107**, 073601 (2011).
 [19] I.-C. Hoi, T. Palomaki, J. Lindkvist, G. Johansson, P. Delsing, and C. M. Wilson, Generation of Nonclassical Microwave States Using an Artificial Atom in 1D Open Space, *Phys. Rev. Lett.* **108**, 263601 (2012).
 [20] K. Reuer, J.-C. Besse, L. Wernli, P. Magnard, P. Kurpiers, G. J. Norris, A. Wallraff, and C. Eichler, Realization of a Universal Quantum Gate Set for Itinerant Microwave Photons, *Phys. Rev. X* **12**, 011008 (2022).
 [21] O. Astafiev, A. M. Zagoskin, A. A. Abdumalikov, Y. A. Pashkin, T. Yamamoto, K. Inomata, Y. Nakamura, and J. S. Tsai, Resonance fluorescence of a single artificial atom, *Science* **327**, 840 (2010).

- [22] A. A. Abdumalikov, O. V. Astafiev, Y. A. Pashkin, Y. Nakamura, and J. S. Tsai, Dynamics of Coherent and Incoherent Emission from an Artificial Atom in a 1D Space, *Phys. Rev. Lett.* **107**, 043604 (2011).
- [23] T. Hönigl-Decrinis, R. Shaikhaidarov, S. E. de Graaf, V. N. Antonov, and O. V. Astafiev, Two-Level System as a Quantum Sensor for Absolute Calibration of Power, *Phys. Rev. Applied* **13**, 024066 (2020).
- [24] Y. Lu, A. Bengtsson, J. J. Burnett, E. Wiegand, B. Suri, P. Krantz, A. F. Roudsari, A. F. Kockum, S. Gasparinetti, G. Johansson, and P. Delsing, Characterizing decoherence rates of a superconducting qubit by direct microwave scattering, *npj Quantum Inf.* **7**, 1 (2021).
- [25] N. Cottet, S. Jezouin, L. Bretheau, P. Campagne-Ibarcq, Q. Ficheux, J. Anders, A. Auffèves, R. Azouit, P. Rouchon, and B. Huard, Observing a quantum Maxwell demon at work, *Proc. Natl. Acad. Sci. U.S.A.* **114**, 7561 (2017).
- [26] M. Naghiloo, D. Tan, P. M. Harrington, J. J. Alonso, E. Lutz, A. Romito, and K. W. Murch, Heat and Work Along Individual Trajectories of a Quantum Bit, *Phys. Rev. Lett.* **124**, 110604 (2020).
- [27] F. Binder, L. A. Correa, C. Gogolin, J. Anders, and G. Adesso, *Thermodynamics in the Quantum Regime*, Fundamental Theories of Physics (Springer, New York, 2018).
- [28] Y. Lu, I. Strandberg, F. Quijandría, G. Johansson, S. Gasparinetti, and P. Delsing, Propagating Wigner-Negative States Generated from the Steady-State Emission of a Superconducting Qubit, *Phys. Rev. Lett.* **126**, 253602 (2021).
- [29] A. Ronzani, B. Karimi, J. Senior, Y.-C. Chang, J. T. Peltonen, C. Chen, and J. P. Pekola, Tunable photonic heat transport in a quantum heat valve, *Nat. Phys.* **14**, 991 (2018).
- [30] J. Senior, A. Gubaydullin, B. Karimi, J. T. Peltonen, J. Ankerhold, and J. P. Pekola, Heat rectification via a superconducting artificial atom, *Commun. Phys.* **3**, 40 (2020).
- [31] Y. Lu, N. Lambert, A. F. Kockum, K. Funo, A. Bengtsson, S. Gasparinetti, F. Nori, and P. Delsing, Steady-state heat transport and work with a single artificial atom coupled to a waveguide: Emission without external driving, *PRX Quantum* **3**, 020305 (2022).
- [32] P. Campagne-Ibarcq, P. Six, L. Bretheau, A. Sarlette, M. Mirrahimi, P. Rouchon, and B. Huard, Observing Quantum State Diffusion by Heterodyne Detection of Fluorescence, *Phys. Rev. X* **6**, 011002 (2016).
- [33] A. N. Jordan, A. Chantasri, P. Rouchon, and B. Huard, Anatomy of fluorescence: Quantum trajectory statistics from continuously measuring spontaneous emission, *Quantum Stud. Math. Found.* **3**, 237 (2016).
- [34] M. Naghiloo, N. Foroozani, D. Tan, A. Jadbabaie, and K. W. Murch, Mapping quantum state dynamics in spontaneous emission, *Nat. Commun.* **7**, 11527 (2016).
- [35] Q. Ficheux, S. Jezouin, Z. Leghtas, and B. Huard, Dynamics of a qubit while simultaneously monitoring its relaxation and dephasing, *Nat. Commun.* **9**, 1926 (2018).
- [36] M. Scigliuzzo, A. Bengtsson, J.-C. Besse, A. Wallraff, P. Delsing, and S. Gasparinetti, Primary Thermometry of Propagating Microwaves in the Quantum Regime, *Phys. Rev. X* **10**, 041054 (2020).
- [37] P. Campagne-Ibarcq, L. Bretheau, E. Flurin, A. Auffèves, F. Mallet, and B. Huard, Observing Interferences between Past and Future Quantum States in Resonance Fluorescence, *Phys. Rev. Lett.* **112**, 180402 (2014).
- [38] D. Tan, N. Foroozani, M. Naghiloo, A. H. Küllerich, K. Mølmer, and K. W. Murch, Homodyne monitoring of postselected decay, *Phys. Rev. A* **96**, 022104 (2017).
- [39] M. Naghiloo, D. Tan, P. M. Harrington, P. Lewalle, A. N. Jordan, and K. W. Murch, Quantum caustics in resonance-fluorescence trajectories, *Phys. Rev. A* **96**, 053807 (2017).
- [40] S. J. Van Enk and H. J. Kimble, On the classical character of control fields in quantum information processing, *Quantum Inf. Comput.* **2**, 1 (2002).
- [41] A. Silberfarb and I. H. Deutsch, Entanglement generated between a single atom and a laser pulse, *Phys. Rev. A* **69**, 042308 (2004).
- [42] W. M. Itano, Comment on “Some implications of the quantum nature of laser fields for quantum computations”, *Phys. Rev. A* **68**, 046301 (2003).
- [43] A. Silberfarb and I. H. Deutsch, Continuous measurement with traveling-wave probes, *Phys. Rev. A* **68**, 013817 (2003).
- [44] H. Nha and H. J. Carmichael, Decoherence of a two-state atom driven by coherent light, *Phys. Rev. A* **71**, 013805 (2005).
- [45] J. Gea-Banacloche and M. Ozawa, Constraints for quantum logic arising from conservation laws and field fluctuations, *J. Opt. B* **7**, S326 (2005).
- [46] P. Bertet, S. Osnaghi, A. Rauschenbeutel, G. Nogues, A. Auffèves, M. Brune, J. M. Raimond, and S. Haroche, A complementarity experiment with an interferometer at the quantum-classical boundary, *Nature (London)* **411**, 166 (2001).
- [47] See Supplemental Material at <http://link.aps.org/supplemental/10.1103/PhysRevLett.129.110601> for information about the experimental setup, detailed calibrations and extended data, which includes Refs. [48–51].
- [48] N. Cottet, H. Xiong, L. B. Nguyen, Y.-H. Lin, and V. E. Manucharyan, Electron shelving of a superconducting artificial atom, *Nat. Commun.* **12**, 6383 (2021).
- [49] F. Pedregosa, G. Varoquaux, A. Gramfort, V. Michel, B. Thirion, O. Grisel, M. Blondel, P. Prettenhofer, R. Weiss, V. Dubourg, J. Vanderplas, A. Passos, D. Cournapeau, M. Brucher, M. Perrot, and E. Duchesnay, Scikit-learn: Machine learning in Python, *J. Mach. Learn. Res.* **12**, 2825 (2011).
- [50] G. Lindblad, On the generators of quantum dynamical semigroups, *Commun. Math. Phys.* **48**, 119 (1976).
- [51] S. Haroche and J.-M. Raimond, *Exploring the Quantum. Atoms, Cavities and Photons*, Oxford Graduate Texts ed. (Oxford University Press, Oxford, 2006).
- [52] C. Macklin, K. O’Brien, D. Hover, M. E. Schwartz, V. Bolkhovskiy, X. Zhang, W. D. Oliver, and I. Siddiqi, A near-quantum-limited Josephson traveling-wave parametric amplifier, *Science* **350**, 307 (2015).
- [53] U. Vool and M. Devoret, Introduction to quantum electromagnetic circuits, *Int. J. Circuit Theory Appl.* **45**, 897 (2017).
- [54] A. A. Clerk, M. H. Devoret, S. M. Girvin, F. Marquardt, and R. J. Schoelkopf, Introduction to quantum noise, measurement, and amplification, *Rev. Mod. Phys.* **82**, 1155 (2010).

- [55] N. Cottet, Energy and information in fluorescence with superconducting circuits, Ph.D. thesis, ENS Paris, 2018.
- [56] H. M. Wiseman, Weak values, quantum trajectories, and the cavity-QED experiment on wave-particle correlation, *Phys. Rev. A* **65**, 032111 (2002).
- [57] M. Tsang, Optimal waveform estimation for classical and quantum systems via time-symmetric smoothing, *Phys. Rev. A* **80**, 033840 (2009).
- [58] S. Gammelmark, B. Julsgaard, and K. Molmer, Past Quantum States of a Monitored System, *Phys. Rev. Lett.* **111**, 160401 (2013).
- [59] M. Maffei, P. A. Camati, and A. Auffèves, Probing non-classical light fields with energetic witnesses in waveguide quantum electrodynamics, *Phys. Rev. Research* **3**, L032073 (2021).
- [60] M. Maffei *et al.* (to be published).
- [61] S. S. Mizrahi and V. V. Dodonov, Creating quanta with an annihilation operator, *J. Phys. A* **35**, 8847 (2002).
- [62] J. Dressel, M. Malik, F. M. Miatto, A. N. Jordan, and R. W. Boyd, Colloquium: Understanding quantum weak values: Basics and applications, *Rev. Mod. Phys.* **86**, 307 (2014).
- [63] H. Ghosh and C. C. Gerry, Measurement-induced non-classical states of the Jaynes–Cummings model, *J. Opt. Soc. Am. B* **14**, 2782 (1997).
- [64] K. A. Fischer, R. Trivedi, V. Ramasesh, I. Siddiqi, and J. Vučković, Scattering into one-dimensional waveguides from a coherently-driven quantum-optical system, *Quantum* **2**, 69 (2018).
- [65] M. Ueda, N. Imoto, H. Nagaoka, and T. Ogawa, Continuous quantum-nondemolition measurement of photon number, *Phys. Rev. A* **46**, 2859 (1992).
- [66] C. M. Nunn, J. D. Franson, and T. B. Pittman, Modifying quantum optical states by zero-photon subtraction, *Phys. Rev. A* **105**, 033702 (2022).
- [67] J.-C. Besse, S. Gasparinetti, M. C. Collodo, T. Walter, A. Remm, J. Krause, C. Eichler, and A. Wallraff, Parity Detection of Propagating Microwave Fields, *Phys. Rev. X* **10**, 011046 (2020).
- [68] R. Dassonneville, R. Assouly, T. Peronnin, P. Rouchon, and B. Huard, Number-Resolved Photocounter for Propagating Microwave Mode, *Phys. Rev. Applied* **14**, 044022 (2020).
- [69] E. Shahmoon, S. Levit, and R. Ozeri, Qubit coherent control and entanglement with squeezed light fields, *Phys. Rev. A* **80**, 033803 (2009).
- [70] A. Z. Goldberg and A. M. Steinberg, Transcoherent states: Optical states for maximal generation of atomic coherence, *PRX Quantum* **1**, 020306 (2020).
- [71] K. Brandner, M. Bauer, M. T. Schmid, and U. Seifert, Coherence-enhanced efficiency of feedback-driven quantum engines, *New J. Phys.* **17**, 065006 (2015).
- [72] J. Yi, P. Talkner, and Y. W. Kim, Single-temperature quantum engine without feedback control, *Phys. Rev. E* **96**, 022108 (2017).
- [73] C. Elouard, D. Herrera-Martí, B. Huard, and A. Auffèves, Extracting Work from Quantum Measurement in Maxwell’s Demon Engines, *Phys. Rev. Lett.* **118**, 260603 (2017).
- [74] C. Elouard and A. N. Jordan, Efficient Quantum Measurement Engines, *Phys. Rev. Lett.* **120**, 260601 (2018).
- [75] X. Ding, J. Yi, Y. W. Kim, and P. Talkner, Measurement-driven single temperature engine, *Phys. Rev. E* **98**, 042122 (2018).
- [76] K. Abdelkhalek, Y. Nakata, and D. Reeb, Fundamental energy cost for quantum measurement, [arXiv:1609.06981](https://arxiv.org/abs/1609.06981).
- [77] L. Buffoni, A. Solfanelli, P. Verrucchi, A. Cuccoli, and M. Campisi, Quantum Measurement Cooling, *Phys. Rev. Lett.* **122**, 070603 (2019).
- [78] A. Solfanelli, L. Buffoni, A. Cuccoli, and M. Campisi, Maximal energy extraction via quantum measurement, *J. Stat. Mech.* (2019) 094003.
- [79] S. Seah, S. Nimmrichter, and V. Scarani, Maxwell’s Lesser Demon: A Quantum Engine Driven by Pointer Measurements, *Phys. Rev. Lett.* **124**, 100603 (2020).
- [80] L. Bresque, P. A. Camati, S. Rogers, K. Murch, A. N. Jordan, and A. Auffèves, Two-Qubit Engine Fueled by Entanglement and Local Measurements, *Phys. Rev. Lett.* **126**, 120605 (2021).
- [81] S. K. Manikandan, C. Elouard, K. W. Murch, A. Auffèves, and A. N. Jordan, Efficiently fueling a quantum engine with incompatible measurements, *Phys. Rev. E* **105**, 044137 (2022).
- [82] F. Campaioli, F. A. Pollock, F. C. Binder, L. Céleri, J. Goold, S. Vinjanampathy, and K. Modi, Enhancing the Charging Power of Quantum Batteries, *Phys. Rev. Lett.* **118**, 150601 (2017).
- [83] D. Ferraro, M. Campisi, G. M. Andolina, V. Pellegrini, and M. Polini, High-Power Collective Charging of a Solid-State Quantum Battery, *Phys. Rev. Lett.* **120**, 117702 (2018).
- [84] F. C. Binder, S. Vinjanampathy, K. Modi, and J. Goold, Quantacell: Powerful charging of quantum batteries, *New J. Phys.* **17**, 075015 (2015).
- [85] G. M. Andolina, M. Keck, A. Mari, M. Campisi, V. Giovannetti, and M. Polini, Extractable Work, the Role of Correlations, and Asymptotic Freedom in Quantum Batteries, *Phys. Rev. Lett.* **122**, 047702 (2019).
- [86] S. Julià-Farré, T. Salamon, A. Riera, M. N. Bera, and M. Lewenstein, Bounds on the capacity and power of quantum batteries, *Phys. Rev. Research* **2**, 023113 (2020).
- [87] F. Caravelli, B. Yan, L. P. García-Pintos, and A. Hamma, Energy storage and coherence in closed and open quantum batteries, *Quantum* **5**, 505 (2021).
- [88] S. Tirone, R. Salvia, and V. Giovannetti, Quantum Energy Lines and the Optimal Output Ergotropy Problem, *Phys. Rev. Lett.* **127**, 210601 (2021).